Relative Navigation and Docking of an sUAS and an UGV

Maarten Uijt de Haags Christian Berth
Technische Universität Berlin (TU Berlin)
Marchstrasse 12, 10587 Berlin
GERMANY

maarten.uijtdehaag@tu-berlin.de

ABSTRACT

This paper focusses on the relative navigation problem between a single UAS and UGV and specifically addresses navigation during the approach and landing procedures. The sensor integration method is based on sensor payload that consists of a Global Navigation Satellite System (GNSS) sensor, an inertial measurement unit (IMU), a laser-altimeter sensor, range radios (RR) and a down-ward looking vision sensor (i.e., camera). This sensor payload can exchange the raw sensor measurements between both platforms. During regular operations, the relative position and velocity is estimated using the GNSS pseudorange and carrier-phase measurements integrated with IMU data and RR data for robustness purposes (i.e., to meet the required assurance levels to maintain safe separation), during approach and landing, however, the GNSS/Inertial solutions is augmented with a laser altimeter for altitude and either RR or a vision-based system that uses camera images of the landing platform to measure the lateral deviations. This paper outlines the underlying methodology and integration mechanizations, some simulation results, and the platform software and hardware setup. It furthermore analyses and discusses the navigation performance using UAS/UGV flight simulation data.

1.0 INTRODUCTION

Both unmanned aerial vehicle (UAV) and unmanned ground vehicles (UGV) are increasingly used for missions that are dull, dirty, dangerous or missions that occur in denied environments (e.g., areas hard to get to by personnel such as disaster zones) [1]. Example applications include environmental monitoring, infrastructure inspection, firefighting, mapping, agriculture, aerial photography, search and rescue, surveillance, and law enforcement, to name a few. UAVs and UGVs each have their own advantages including the longer endurance, larger payload, resilience to environmental conditions and 2D operation for UGVs, and larger field-of-view, flexible vantage point, reduced size, increased manoeuvrability and speed and 3D operation for UAV. Collaboration between an UAV and an UGV would, therefore, be the optimal solution for many of the applications areas (see for example Figure 1-1).

Many approaches can be found in the literature to land an UAV in a predefined location or on a UGV either stationary or moving. In general, the solutions consist of (i) a relative position estimation, (ii) an approach to generate a pursuit trajectory, (iii) and the flight control required to track this generated trajectory to the landing location where the UAV will be docked on the UGV. The focus in this paper will be on the relative position capabilities, but the interface to the other two functions will be illustrated later.

For most commercial UAVs, Global Navigation Satellite Systems (GNSS) including the U.S. Global Positioning System (GPS) and Europe's Galileo, have become one of the most dependable sources for absolute on-board position and velocity information enabling very stable position control of the UAV operating in autonomous or semi-autonomous modes.

Figure 1-1: Interaction of ground and aerial vehicles.

In regular aviation GPS-based position and velocity estimates are broadcast by general and commercial aircraft equipped with Automatic Dependent Surveillance-Broadcast (ADS-B) along with an estimate of their accuracy and integrity: Navigation Accuracy Category for position/velocity (NACp/NACv), Navigation Integrity Category (NIC) and Source Integrity Level (SIL) [2]. Based on information received from ADS-B an aircraft can determine its separation vector in the navigation coordinate frame and use the relative position and velocity to assess if a future loss-of-separation will occur. The position source in ADS-B is typically a Standalone-GPS receiver (with or without onboard integrity monitor), a Space-based Augmentation System receiver (SBAS), or in case the ground infrastructure is available a Ground-based Augmentation (GBAS) solution, the latter two providing better accuracy and integrity. Alternative ADS-B solutions have been investigated to obtain an improved accuracy and integrity with an unaugmented solution using the exchange of raw GPS measurements between two aircraft [3]. This system was also used and demonstrated on UAVs using other means of communication to exchange the data [4]. The latter system could be used for UAV/UGV relative positioning and will be discussed later in this paper.

GNSS has been used in estimating the relative baseline between UAV and UGV. For example, [5] uses Real-Time Kinematic (RTK) GPS in combination with an Inertial Measurement Unit (IMU) onboard both the UAV (fixed wing in their case) and the UGV. In RTK, the onboard receiver (i.e., rover) uses the highly accurate GPS carrier-phase measurements in combination with corrections from a base station in the vicinity of the platform to obtain a cm-level position estimate of the rover [6]. Typically, RTK equipment is expensive, although that has been changing, and require a base station.

In many environments where a cooperative UAV/UGV would operate, GNSS performance is degraded or even unavailable. These environments are typically referred to as GNSS-denied or semi-denied environments and include urban environments, under-the-canopy, indoor and interference/jamming/spoofing environments. In these environments, the UAV and UGV must be able to depend on alternative navigation methods including (a) integration of GNSS with IMU [7], (b) the integration of inertial sensors with imagery and laser scanners [8], (c) beacon-based navigation (i.e., pseudolites, Ultra-wide band or UWB) [8], (d) or navigation using signals of opportunity [9].

Many approaches in the literature use camera imagery to estimate the relative position between the UAV and UGV especially when both are in close range. For example, in [10], the UAV takes a picture of the take-off location, and, upon return uses this image as a reference to determine the position of the UAV with respect to the landing location. More popular is the use of fiducial markers or fiducials installed on the UGV. Fiducial markers are objects placed on the UGV that are used as reference points. These objects typically consist of

unique patterns that can be found and uniquely identified by the onboard vision system and used to estimate the relative pose (i.e., position and attitude) of the observer with respect to the pattern. Examples of more complex fiducial markers are AprilTags [11], ArUco markers [12] and STags [13] (see Figure 1-2 for examples).

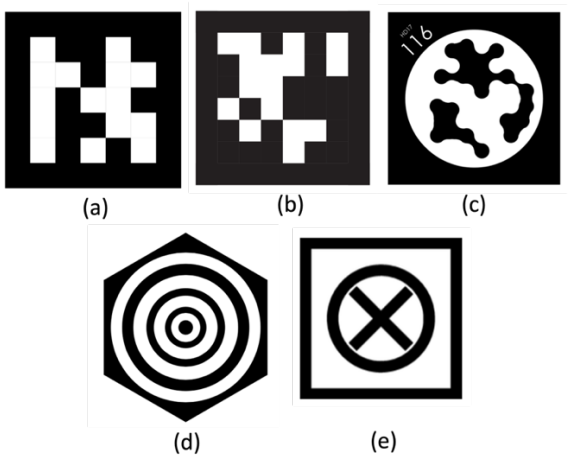

Figure 1-2: Marker examples: (a) ArUco maker, (b) Apriltag, (c) STags.

Fiducial markers such as the latter three can be used to obtain an estimate of the relative pose, i.e., the relative position and orientation with respect to the marker (see Figure 1-3 left). The performance of these estimators has been evaluated for various fiducial markers in [13] and [14] with the above ArUco, AprilTag and STag outperforming various others. Typical translation errors are on the order of cm's for distances up to 3m and viewing angles up to 80^0, whereas angular errors were at the multiple-degree level.

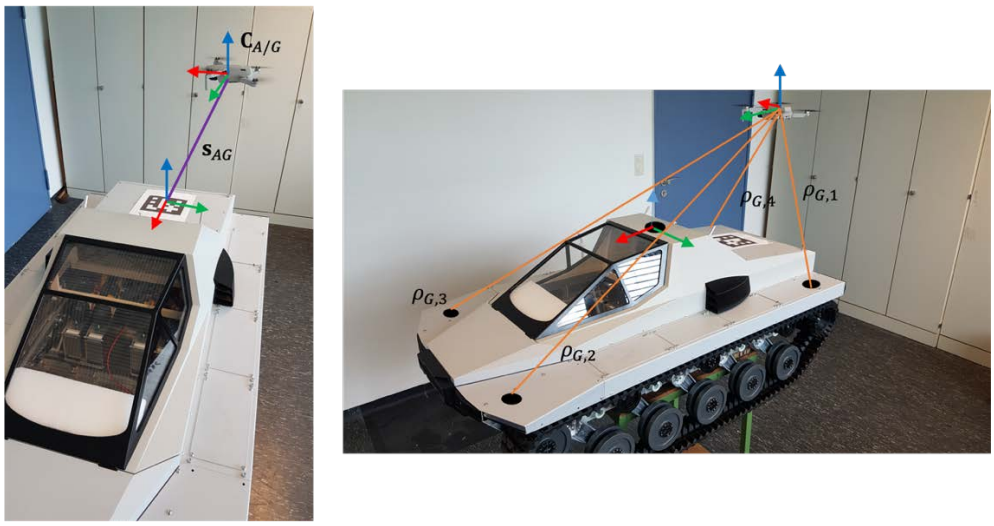

Figure 1-3: Relative pose (i.e., position and orientation) of UAV with respect to marker on the UGV; Using fiducial marker(s) (left); using UWB range measurements (right).

In [15], a UAV was equipped with a fish-eye lens camera and the ground vehicle with a large red rectangle. The UAV detects the rectangle using blob detection and uses this information to guide the UAV to the target area. The marker shown in Figure 1-2d was used by the authors in [16]. Knowledge of the ring dimension is

used to estimate height and the distance between the camera center and the location of the rings in the image is used to estimate the lateral displacement. The authors in [17] propose a system that estimates the UAV state using visual odometry and a marker (see Figure 2-1e) to detect and estimate the state of the target platform using a Kalman filter. Based on their predicted relative state, a UAV trajectory is planned and tracked by the controller. In [18] an autonomous landing approach on a moving vehicle is proposed using, once again, the maker from Figure 2-1e to track the ground vehicle. However, in this case, the authors also included information from a highly accurate RTK GPS solution in the UAV state estimator. In both [17] and [18] an accurate dynamics model of the ground vehicle was incorporated in the ground vehicle state estimator. Other relative pose estimation examples using AprilTags include the landing of a UAV on a ship at sea [19], the landing on a high speed (i.e., 50km/h) vehicle [20], and landing of a UAV under high wind conditions [21]. The UAV state estimator in [20] also incorporates data from a GPS and IMU from a mobile phone. Finally, examples of using ArUco marker are discussed in [22] and [23].

Alternative vision-based methods include the use of an active infrared (IR) beacon located on the UGV and a IR-sensitive camera onboard that can use that beacon to home in on the UGV [24]. Another approach described in [25] uses a 3D imager that is capable of simultaneously obtaining a monochrome image and a corresponding 3D point cloud of the environment. The procedure consists of detecting a unique 3D docking port onboard the UGV and estimating the relative a pose with respect to that port. With the increase in availability of new 3D imaging sensors such as the Intel Realsense sensor, the Occipital Structure, the ZED stereo camera and various other stereo-vision products, the approach in [25] may become more feasible. Possible updates could include the use of a better fiducial such as the ArUco marker or the Apriltag in corporation with the uniquely shaped docking port.

One of the methods that will be introduced in this paper and evaluated using simulation is the use of range radios (RR) such as ultra-wideband (UWB) radios. Use of range radios in UAV swarms for navigation purposes has already been demonstrated in [26] and [27]. The latter development formed the basis for the UWB implementation in our UAV sensor board discussed in Section 3.0.

The next section will describe the proposed architecture followed by a description of its implementation using TU Berlin aerial and ground vehicle. Finally, some simulation results will be shown and plane for flight testing outlined.

2.0 METHODOLOGY

The research platform that is being developed at the TU Berlin Chair for Flight Guidance is meant to support research on relative UAV/UGV navigation during collaborative missions with the ability of the UAV to land on the UGV. An illustration of one possible test scenario is shown in Figure 2-1. For our initial demonstrator, both vehicles will be equipped with GNSS receivers, IMUs, range radios and beacons, vision systems, fiducial markers, and communication equipment.

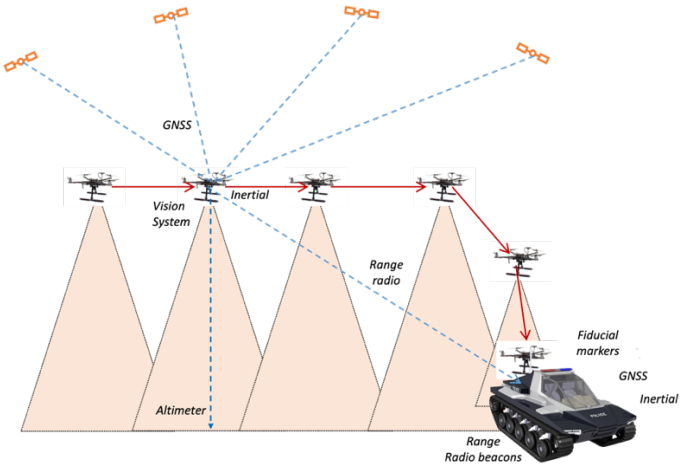

Figure 2-1: Possible test scenario of TUB research setup.

The basic processing approach is shown in Figure 2-2. This block diagram resembles the model of situational awareness in dynamic decision system as introduced by Endsley [28]. Even though Endsley's work focusses on Human Factors, the concept of situational awareness of a human can be easily translated to a situational awareness model of the UAV/UGV relative navigation problem. The decision-making loop shown in Figure 2-2 also shows a lot of similarities with the Observe, Orient, Decide and Act (OODA) loop by Boyd and the perception-action cycle.

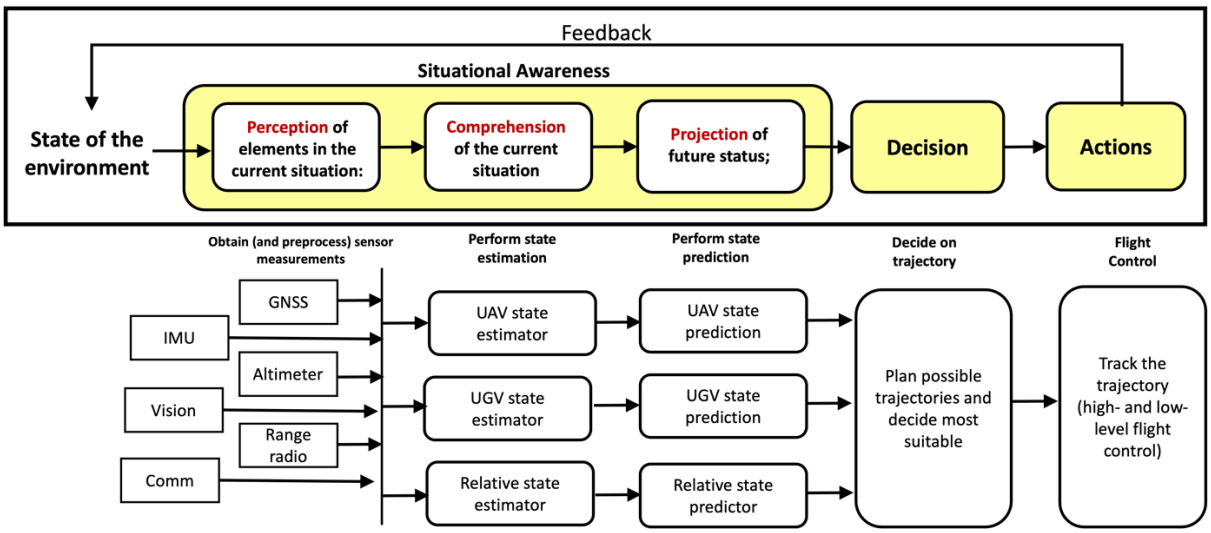

Figure 2-2: Information processing, decision making and action loop.

The first part of the dynamic decision system consists of the perception module where data from the various sensors are collected and pre-processed if necessary. This sensor data consists of the onboard sensor data from the UAV's GNSS receiver, the IMU, the range radio and vision system, and the data received from the UGV via the datalink. Examples of pre-processing are feature extraction and association methods or visual odometry algorithms in the vision system. Once this data has been collected, the system tries to comprehend the current state of the system by estimating the UAV state (position, velocity, attitude, etc.) and, if the UGV has been detected, the UGV state. Alternatively, some methods directly estimate the relative state of both vehicles. These state estimates are then stored in local memory to maintain a history of the UAV and UGV trajectories.

Since the UAV is trying to pursue the UGV and land on it, it is essential to get a good understanding of the future state of the UAV/UGV configuration. Hence, methods are implemented to predict the UAV, UGV and/or relative state based on current and stored trajectories. Based on these predictions, the UAV can calculate potential trajectories to the landing location and identify the optimal one. This trajectory must then be tracked by the flight controller. Many control strategies have been proposed some of which are discussed in the references of Section 1. Another approach would be to use Model Predictive Control as it considers the predicted future state of the system. Example of this approach are discussed in [29] and [30].

To perform the relative state estimation functions, one must consider what information is being transmitted from the UGV to the UAV, if any. This information may include position ($\mathbf{r}_A$ for UAV, $\mathbf{r}_G$ for UGV) and velocity ($\mathbf{v}_A$ for UAV, $\mathbf{v}_G$ for UGV) reports as is typical in manned aviation ADS-B or "raw" sensor measurements like GNSS pseudoranges ($\rho_{A,k}, \rho_{G,k}$) and carrier-phase measurements ($\phi_{A,k}, \phi_{G,k}$), range radio ranges ($r_{A,n}$), and relative pose from fiducial markers ($\mathbf{r}_{AG}, \mathbf{C}_{A/G}$). These measurements can then be used in the estimators onboard the UAV. Examples of what this could look like for various integration strategies (i.e., what sensor information to combine) are listed in Table 2-1. In some cases, no communication between UAV and UGV is necessary. For example, for in case of range radios and fiducial markers only knowledge of the location of these beacons are markers is required.

Table 2-1: Source and associate data.

	Source	With communication		Without communication
		Position/velocity reports	*Measurements/corrections*	
A	INS/Altimeter	$\tilde{\mathbf{r}}_A, \tilde{\mathbf{v}}_A, \tilde{\mathbf{r}}_G, \tilde{\mathbf{v}}_G$	-	-
B	GNSS	$\tilde{\mathbf{r}}_A, \tilde{\mathbf{v}}_A, \tilde{\mathbf{r}}_G, \tilde{\mathbf{v}}_G$	-	-
C	GNSS/INS (EKF)	$\tilde{\mathbf{r}}_A, \tilde{\mathbf{v}}_A, \tilde{\mathbf{r}}_G, \tilde{\mathbf{v}}_G$	-	-
D	GNSS SBAS*	$\tilde{\mathbf{r}}_A, \tilde{\mathbf{v}}_A, \tilde{\mathbf{r}}_G, \tilde{\mathbf{v}}_G$	-	-
E	GNSS SBAS CSC*	$\tilde{\mathbf{r}}_A, \tilde{\mathbf{v}}_A, \tilde{\mathbf{r}}_G, \tilde{\mathbf{v}}_G$	-	-
F	Interferometry*	-	$\rho_{A,k}, \rho_{G,k}$	-
G	Interferometry CSC*	-	$\rho_{A,k}, \phi_{A,k}, \rho_{G,k}, \phi_{G,k}$	-
H	RTK Float	-	$\rho_{A,k}, \rho_{G,k}$	-
I	RTK Fixed	-	$\rho_{A,k}, \phi_{A,k}, \rho_{G,k}, \phi_{G,k}$	-
J	UWB	-	-	$r_{A,n}$
K	UWB/Altimeter (EKF)	-	$r_{A,n}, h_A, h_G$	$r_{A,n}, h_A$
L	UWB/Altimeter (PF)	-	$r_{A,n}, h_A, h_G$	$r_{A,n}, h_A$
M	Fiducial marker	-	$\tilde{\mathbf{r}}_{AG}, \tilde{\mathbf{C}}_{A/G}$	$\tilde{\mathbf{r}}_{AG}, \tilde{\mathbf{C}}_{A/G}$
⋮	⋮	⋮	⋮	⋮

In case of position and velocity reports, the separation vector ($\mathbf{s}_{AG}$) and relative velocity ($\mathbf{v}_{AG}$) can be obtained directly if all vectors are expressed in a common Cartesian frame (e.g., Earth-Centered-Earth-Fixed) and time-aligned:

$$\mathbf{s}_{AG}(t_k) = \mathbf{r}_A(t_k) - \mathbf{r}_G(t_k) \tag{1}$$

$$\mathbf{v}_{AG}(t_k) = \mathbf{v}_A(t_k) - \mathbf{v}_G(t_k) \tag{2}$$

To reduce the noise and to implement a straightforward way to obtain predictions of the UAV/UGV states, a Kalman Filter or Extended Kalman Filter can be implemented based on the appropriate measurement and dynamics equations. The basic steps of the EKF are summarized in equations (3) through (9), but for details of the EKF, the reader is referred to one of the many texts such as [31].

System: dynamics model

$$\mathbf{x}(t_k) = \mathbf{g}[\mathbf{x}(t_{k-1})] + \mathbf{w}(t_k) \tag{3}$$

System: measurement model

$$\mathbf{z}(t_k) = \mathbf{h}[\mathbf{x}(t_k)] + \mathbf{v}(t_k) \tag{4}$$

Kalman filter: update step

$$\hat{\mathbf{x}}(t_k) = \hat{\mathbf{x}}^-(t_k) + \mathbf{K}_k[\mathbf{z}_k(t_k) - \mathbf{h}[\hat{\mathbf{x}}^-(t_k)]] \tag{5}$$

$$\mathbf{K}(t_k) = \frac{\mathbf{P}^-(t_k)\mathbf{H}^T}{[\mathbf{H}(t_k)\mathbf{P}^-(t_k)\mathbf{H}^T(t_k) + \mathbf{R}]} \tag{6}$$

$$\mathbf{P}(t_k) = [\mathbf{I} - \mathbf{K}(t_k)\mathbf{H}(t_k)]\mathbf{P}^-(t_k) \tag{7}$$

Kalman filter: prediction step

$$\hat{\mathbf{x}}^-(t_k) = \hat{\mathbf{x}}(t_k) + \int_{t_{k-1}}^{t_k} \mathbf{g}(\hat{\mathbf{x}}, t)dt \tag{8}$$

$$\mathbf{P}^-(t_k) = \mathbf{\Phi}(t_{k-1})\mathbf{P}(t_{k-1})\mathbf{\Phi}^T(t_{k-1}) + \int_{t_{k-1}}^{t_k} \mathbf{\Phi}(t_{k-1}|t)\mathbf{Q}(t_{k-1})\mathbf{\Phi}^T(t_{k-1}|t)dt \tag{9}$$

where $\boldsymbol{v}_k$ and $\mathbf{w}_k$ are the measurement and process noise, respectively.

Since the state vector in (1) is equal to the separation vector, the measurement equation is linear and **h** can be replaced my matrix **H.** However, the dynamics model is dependent on the vehicles' motion model (UAV and UGV) and can very well be a non-linear function. In that case, the dynamics model **g** must be linearized to obtain state propagation matrix **Φ** that can be used in the EKF. The prediction can be easily obtained by propagating the state prediction in and its covariance in equations (8) and (9) to N time epochs in the future to $\hat{\mathbf{x}}^-(t_{k+N})$ and $\mathbf{P}^-(t_{k+N})$.

3.0 PLATFORM DESCRIPTION

The UAV/UGV research setup at the TU Berlin consists of the XTrack UGV and a modified Holybro S500 UAV. The XTrack seen in Figure 1-3 and Figure 3-1 is a versatile electrically powered track vehicle developed by the TU Berlin Chair of Flight Guidance and Air Traffic and is usable in a wide variety of operational environments. The rubber tracked chassis enables high speeds on land and in the water with very high off-road mobility as well as low ground contact pressure and high driving comfort. Due to the low contact pressure the vehicle allows for operation in an urban environment. The front of the vehicle can also be outfitted with standard attachment systems (plough blade, etc.). The electric drive ensures low-maintenance and very reliable emission-free propulsion. For the planned tests the vehicle is equipped with fiducial markers (see, for example, Figure 1-3), UWB beacons and a GNSS/INS system.

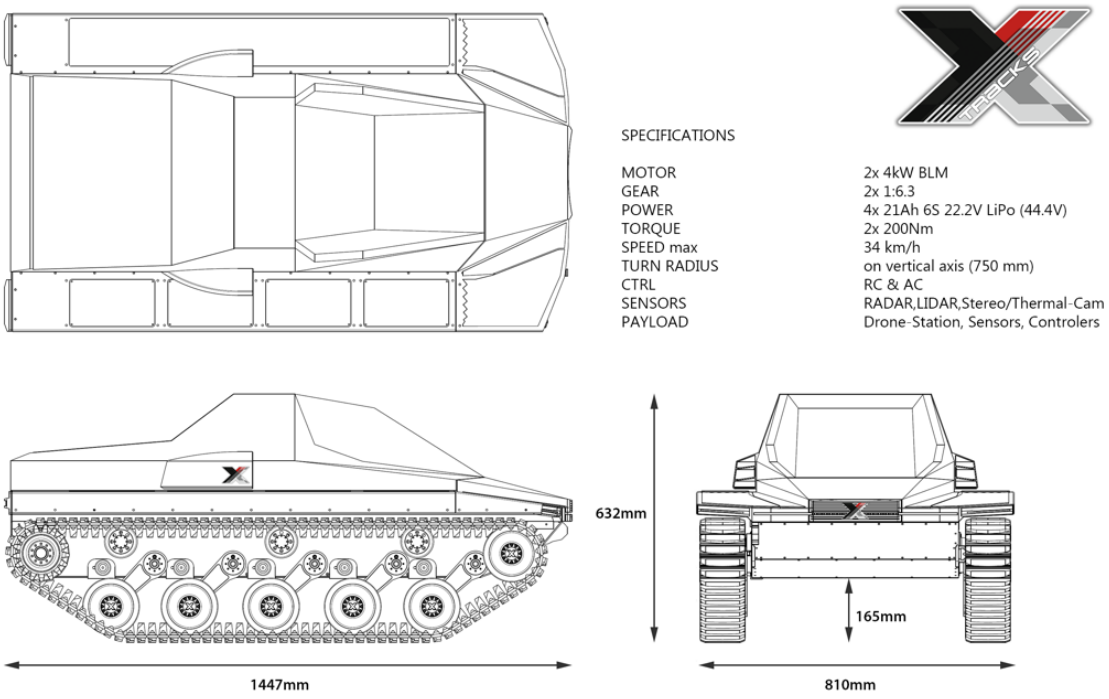

Figure 3-1: X-Track UGV.

Although, a platform the size of the DJI Mavic Mini 2 as depicted in Figure 1-3 would be preferrable, the goal of the test setup is to evaluate a variety of sensor integration approaches for relative navigation and landing. Hence, an UAV with more payload has been chosen: the Holybro S500. This UAV is shown in Figure 3-2 on the left. A block diagram of the payload is shown on the right and includes a mvBlueFOX-MLC202bG monochrome global shutter camera with a 1280x960 resolution, an UTM-20LX laser range scanner (~20m range), a TF03 laser range finder (~100m range), and a custom GNSS/Inertial/UWB board. These sensors are interfaced to a Raspberry Pi 4 (RPi4) running Ubuntu 18.04 and the Robotic Operating System 2 (ROS2). An PX4 Mini was used for flight control purposes with a built-in GPS receiver, baro-altimeter and IMUs for standard operations and a connection to the RPi4 for experimental operations where the algorithms-under-test implemented in the RPi4 are used for navigation. Note that a Jetson Nano is also available but not currently installed.

The GNSS/Inertial/UWB was developed in-house and consists of a u-blox F9T, a multi-frequency multi-constellation and SBAS capable GNSS receiver, an xsens MTi-7 IMU (GNSS/IMU ready) and a Decawave 1000 UWB transceiver. These sensors are interfaced to an STM32 microcontroller that takes care of pre-processing, time-tagging and the interface with the RPi4 via USB. A picture of this board and its block diagram are shown in Figure 3-3.

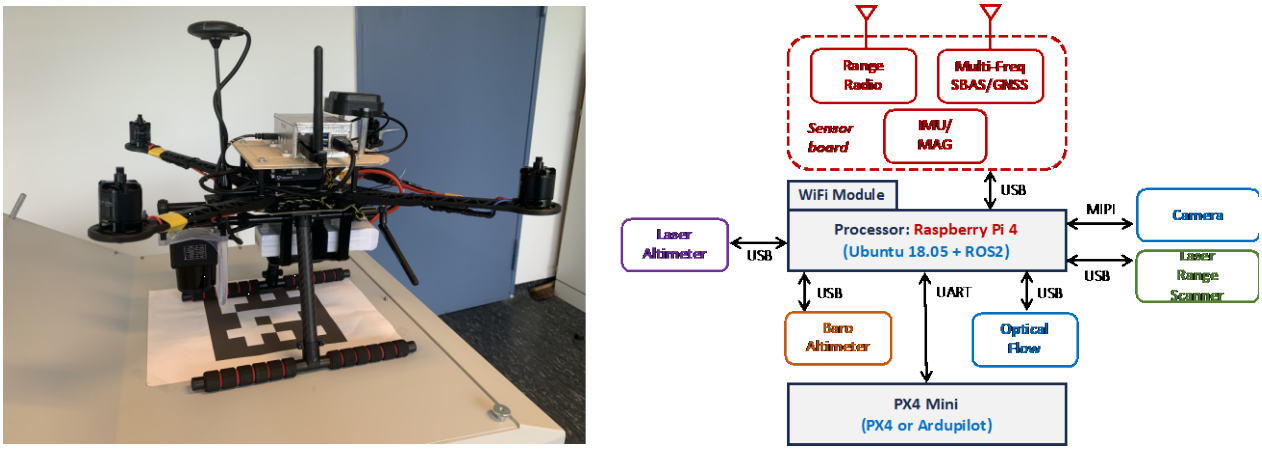

Figure 3-2: Modified Holybro S500 UAV.

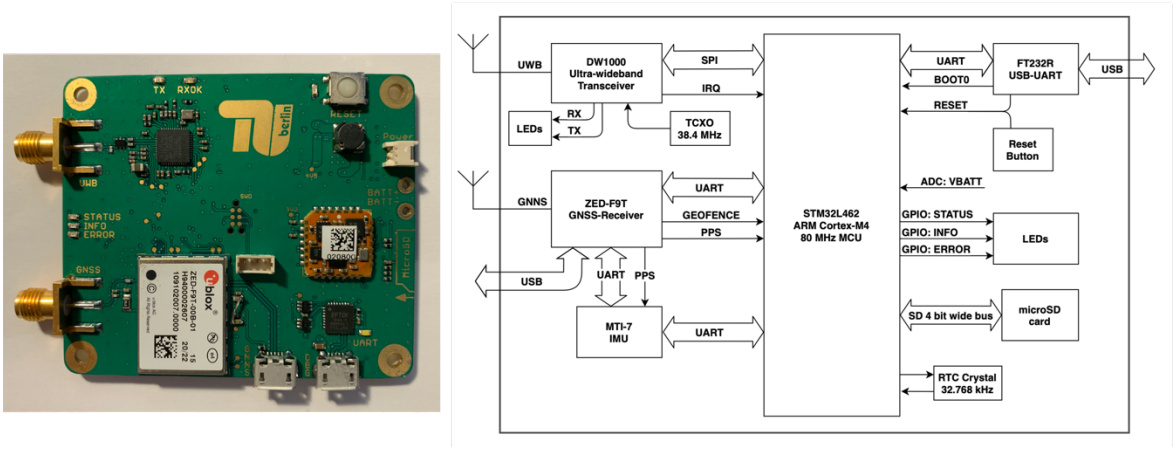

Figure 3-3: GNSS, Inertial, Range-radio board.

4.0 GNSS AND RANGE-RADIO MECHANIZATIONS

4.1 GNSS PVT estimation

As shown in Table 2-1, the GNSS measurements can be used in various manners each with its own navigation performance. The performance difference between the various methods depends on what measurements are used and how tries to mitigate the error. This is driven by the error equations for both the pseudorange, and the carrier-phase measurements are:

$$\rho_j = R_j + c\delta t_u + \delta R_{iono} + \delta R_{tropo} + \delta R_{PR,noise} + \delta R_{PR,mp} + \delta R_{PR,hw} \; - c\delta t_{SV,j} \qquad (10)$$

$$\phi_j = R_j + N_j\lambda + \; c\delta t_u - \delta R_{iono} + \delta R_{tropo} + \delta R_{ID,noise} + \delta R_{ID,mp} + \delta R_{ID,hw} \; - c\delta t_{SV,j} \qquad (11)$$

where R_j is the true range to satellite 'j' given by:

$$R_j + c\delta t_u = \left\| \mathbf{r}_A - \mathbf{r}_{SV_j} \right\| + c\delta t_u \tag{12}$$

$c\delta t_u$ is the receiver clock error, $\delta R_{iono}, \delta R_{tropo}$ are the atmospheric errors, $\delta R_{X,mp}$ is the multipath error, $\delta R_{X,hw}$ is a hardware delay error, $c\delta t_{SV,j}$ are the orbital and satellite clock errors, and $\delta R_{X,noise}$ is the noise error (mm-level for carrier-phase, dc-level for pseudorange). $N_j\lambda$ is an unknown integer ambiguity that causes the carrier to have an offset from the pseudorange. This unknown bias is constant unless cycle slips occur due to excessive dynamics of the receiver or low signal strength (among others).

In standalone GNSS, the position is typically estimated using an ordinary least square (OLS), a weighted least square (WLS) or an EKF, where the range equation in equation (12) is linearized (see [33]). To further improve navigation performance, a differential operation can be implemented. In this mode of operation, measurements are made by one or more receivers in a known location and errors are estimated. These error estimates are then transmitted to the users using a geo-stationary satellite (SBAS), a VHF datalink (GBAS) or via commercial services. In this case all the spatially correlated errors in (10) and (11) can be mitigated. Errors like the noise and multipath, however, are spatially uncorrelated and can, therefore, not be reduced. However, as the carrier-phase measurements have a much lower noise, they can be used to smooth the noisier pseudorange measurement using carrier-smoothed code (CSC):

$$\rho_{i,csc}(t_k) = \frac{N-1}{N}\left\{\rho_{i,csc}(t_{k-1}) + \phi_i(t_k) - \phi_i(t_{k-1})\right\} + \frac{1}{N}\rho_i(t_k) \tag{13}$$

where N is the smoothing time. These smoothed pseudoranges can then be used again to determine the UAV or UGV position using the OLS, WLF or EKF.

Real-time kinematic (RTK) processing techniques require a ground station and perform ambiguity resolution techniques to estimate the integer ambiguity and baseline between the user and the ground station. These methods typically implement single and double difference techniques to reduce the other error sources [33].

In addition to GNSS-only techniques, the GNSS measurements can also be integrated with IMUs. One such method that we have implemented is the tight integration method introduced in [7]. This method consists of a separate dynamics filter that uses sequential carrier-phase measurements to estimate the IMU errors (velocity drift, tilt, accel and gyro bias errors), and a position error that calculated the position based on the pseudoranges and the outputs of the dynamics filter.

In all above approaches, the UAV and the UGV compute their position and velocity and broadcast position and velocity reports. Alternatively, the UAV and UGV can exchange raw GNSS measurements (i.e., pseudoranges and carrier-phase measurements). Given the raw measurements from both target and ownship, range single differences, SD (difference between measurement from UAV and UGV), double differences, DD (difference of SDs with respect to a key satellite), and sequential (triple) differences can be used to accurately derive the separation vector or relative position vector between ownship and traffic as well as the change in separation vector. The latter quantity is directly related to the average velocity over a time epoch. The geometry for this scenario is illustrated in Figure 4-1.

The advantages of using a *raw measurement-based* approach rather than a *position-based* approach is that the former method (i) exploits well-established pseudorange double difference techniques, (ii) exploits well-established carrier-phase sequential difference techniques, (iii) improves the accuracy by the inherent removal of spatial and temporally correlated errors in double- and sequential differencing, (iv) increases observability

by having both the measurements from the target and ownship, (v) is independent of a Datum Reference (e.g., coordinate frame is chosen by the sUAS using the measurement to calculate the position), (vi) always accounts for correlations (both spatial and temporal), (vii) can perform optimal weighting of the measurements in the position and velocity estimates, (viii) and can implement common GNSS integrity methods such as RAIM [3].

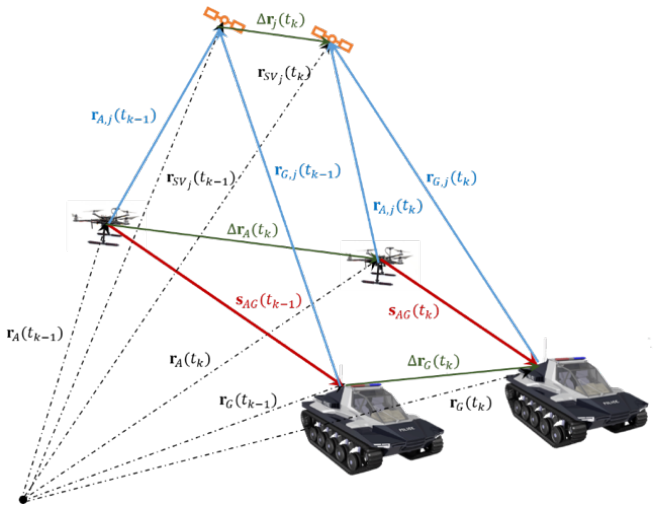

Figure 4-1: Relative position and velocity scenario for UAV and UGV.

Figure 4-2 summarizes the structure of the relative position and velocity estimation algorithm using GNSS raw measurements and its associated mathematics.

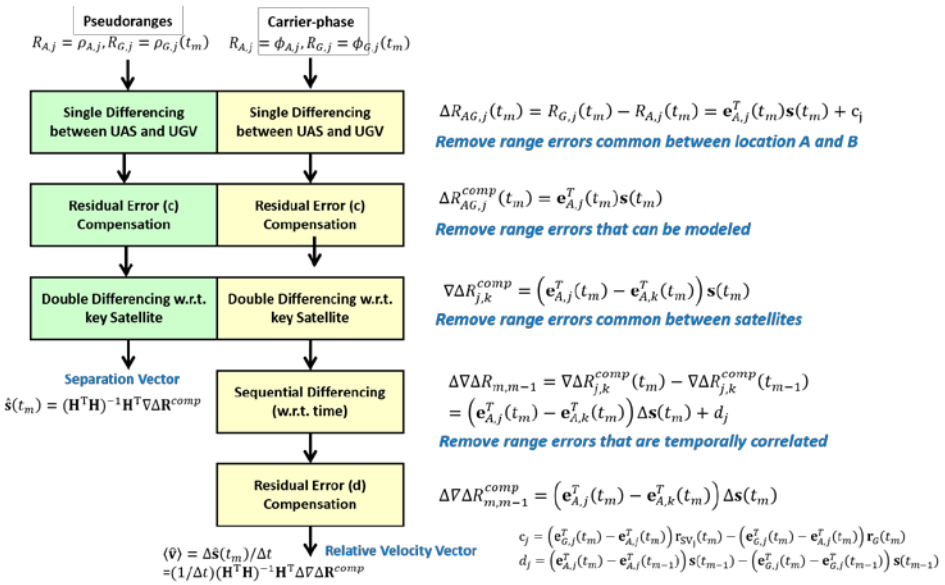

Figure 4-2: GNSS-based relative position and velocity estimation.

The summary in Figure 4-2 is given for a set of general ranges to the satellites **R**. In our implementation, the separation vector is derived using the GNSS pseudorange measurements in vector **ρ**, or

$$\hat{\mathbf{s}}(t_m) = \left(\mathbf{H}^{\mathrm{T}} \cdot \mathbf{H}\right)^{-1} \mathbf{H}^{\mathrm{T}} \cdot \nabla\Delta\rho^{comp} \tag{14}$$

The relative velocity vector is estimated using solely the carrier-phase measurements:

$$\hat{\mathbf{v}} = \frac{1}{t_k - t_{k-1}} (\mathbf{H}^{\mathrm{T}} \cdot \mathbf{H})^{-1} \mathbf{H}^{\mathrm{T}} \cdot \Delta\nabla\Delta\boldsymbol{\varphi}^{comp} \tag{15}$$

Rather than using CSC, one could also formulate a filter that combines the relative position (i.e., separation vector) estimate with the relative velocity estimate of equation, in a manner like the CSC:

$$\mathbf{s}_{filt}(t_m) = (1 - K)\hat{\mathbf{s}}^n(t_k) + K\left[\mathbf{s}^n_{filt}(t_{k-1}) + \Delta\hat{\mathbf{s}}^n(t_k)\right] \tag{16}$$

For both the separation vector and the relative velocity vector LS estimators, a fault detection and exclusion (FDE) method can be formulated to detect off-nominal uncorrelated errors or other threats (e.g., cycle slips).

4.2 Range radio

Range radio beacons have been used for positioning given a set of stationary beacons [27], or integrated with IMU to determine the relative location of swarm members or for indoor localization of these members [26]. In the latter example, a UWB system was developed based on the Decawave 1000 sensor and the following two-way ranging performance was measured for ranges up to 10m.

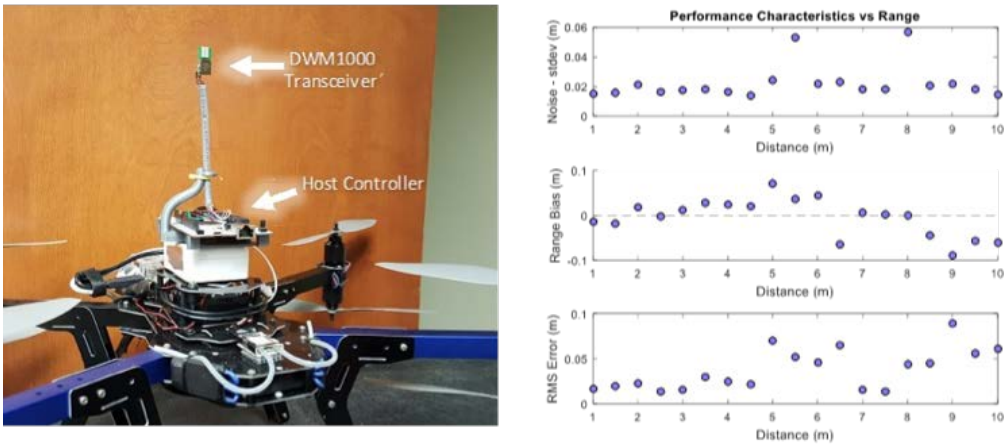

Figure 4-3: UBW range radio prototype and two-way ranging performance for ranges up-to 10m.

In our proposed UWB implementation, the UGV is equipped with UWB beacons on known locations within the UGV's body frame, and the UAV is equipped with a UWB transceiver. The two-range to beacon 'n' is given by:

$$\tilde{r}_{A,n}(t_k) = \left\| \mathbf{r}_A - \mathbf{r}_{G,n} \right\| + v_{uwb} \tag{17}$$

where both positions are expressed in the body frame of the UGV. If one wants to express the relative position in a navigation from (e.g., East-North-Up), then the beacon locations should be aligned with this frame, for example, by having the UGV transmit its orientation in the form of a transformation matrix from body to navigation frame, $\mathbf{C}_b^n$. Then $\mathbf{r}_{G,n} = \mathbf{C}_b^n \mathbf{r}_{G,n}^b$.

$$\mathbf{H} = \begin{bmatrix} \mathbf{e}_{G,1}^T \\ \vdots \\ \mathbf{e}_{G,N}^T \end{bmatrix} \tag{18}$$

where $\mathbf{e}_{G,n}$ is the direction cosine to beacon 'n':

$$\mathbf{e}_{G,n} = \begin{bmatrix} \frac{x_A - x_{G,n}}{\|\mathbf{r}_A - \mathbf{r}_{G,n}\|} & \frac{y_A - y_{G,n}}{\|\mathbf{r}_A - \mathbf{r}_{G,n}\|} & \frac{z_A - z_{G,n}}{\|\mathbf{r}_A - \mathbf{r}_{G,n}\|} \end{bmatrix}^T \tag{19}$$

The WLS estimate can now be obtained using:

$$\hat{\mathbf{x}} = \left(\mathbf{H^T W H}\right)^{-1} \mathbf{H^T W z} \tag{20}$$

where **W** is the diagonal weighting matrix with $1/\sigma_{v_{uwb}}^2$ in the diagonal elements and is the vector with all the **z** range measurements. Since the geometry of this problem can be ill-defined at larger distances to the UGV, it is important to look at the dilution of precision values given by the square root of the sum of the x- and y-coordinate of $(\mathbf{H^T W H})^{-1}$ for the horizontal DOP or HDOP, and the square-root of the z-component for the vertical DOP or VDOP.

To obtain a better solution, the UWB-only solution could be augmented with altimeter measurements. Note that in this case, these measurements must be made with respect to the altitude of the UGV. This means that extra information may be required such as reference pressure (at the UGV location) for a baro-altimeter or terrain information for laser and radar altimeters. Assuming that this has been taken care off, the measurement matrix can be modified as follows:

$$\mathbf{H} = \begin{bmatrix} \mathbf{e}_{G,1}^T \\ \vdots \\ \mathbf{e}_{G,N}^T \\ [0 \quad 0 \quad 1] \end{bmatrix} \tag{21}$$

Note that the measurement matrices in (18) and (21) can also be used in an EKF formation that includes a motion model of the UGV and UAV. Furthermore, a complementary EKF could be formulated when integrating the UWB beacon and altimeter with an IMU.

5.0 SIMULATION SETUP AND RESULTS

Since the actual UAV/UGV test setup described in Section 3.0 was not yet operational at the time of writing of this paper, this section includes the navigation simulation results generated to evaluate the useability of various integration approaches listed in Table 2-1.

5.1 Simulation setup

The simulation was implemented in Matlab and included various scenarios, one of which is shown here to illustrate the performance of the various navigation approaches. The UAV/UGV scenario is shown in Figure 5-1. In this scenario both the UAV (trajectory shown in magenta) and the UGV (trajectory shown in blue) are mobile. After detection of the UGV, the UAV flies an arc at constant altitude, then descents and lines up with the predicted UGV trajectory after which it keeps pace and slowly descents on the UGV platform. Note that the controller details and implementation is not part of the discussion here.

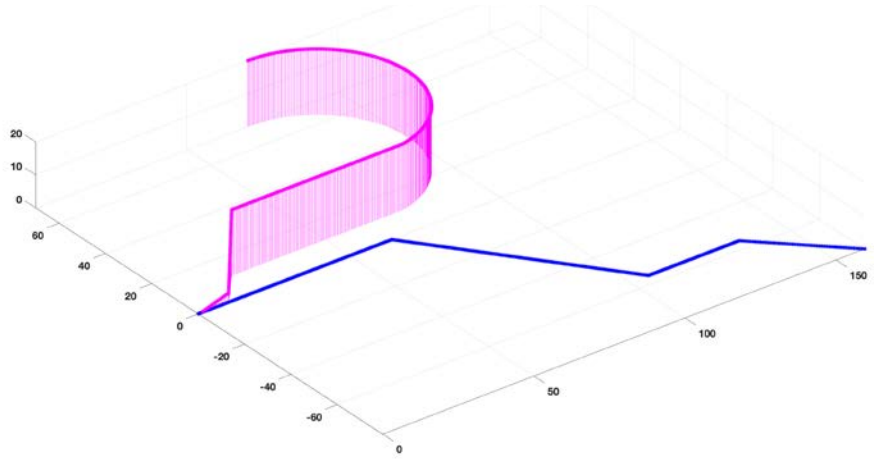

Figure 5-1: Trajectories of the UAV (magenta) and UGV (blue) for the discussed scenario.

5.2 Results

The first set of results is shown in Figure 5-2. Here, the separation vector is calculated according to equation (1) by subtracting the received position report from the ownship position. The left side shows the results using INS outputs (tactical grade INS) as source with a clearly visible drift error. The results on the right side are obtained using standalone pseudorange-based (WLS) GPS. Typical m-level noise levels can be observed with a non-zero mean due to the various slowly varying error sources present in the pseudorange measurements. In the simulation the pseudoranges were simulated based on real ephemeris data with a different set of satellites for the UAV and the UGV. Therefore, the common error does not disappear when subtracting both positions. Clearly, the errors are not sufficient to get close to the UGV's landing pad (which has a dimension of about 60cm-by-60cm for the XTrack vehicle simulated).

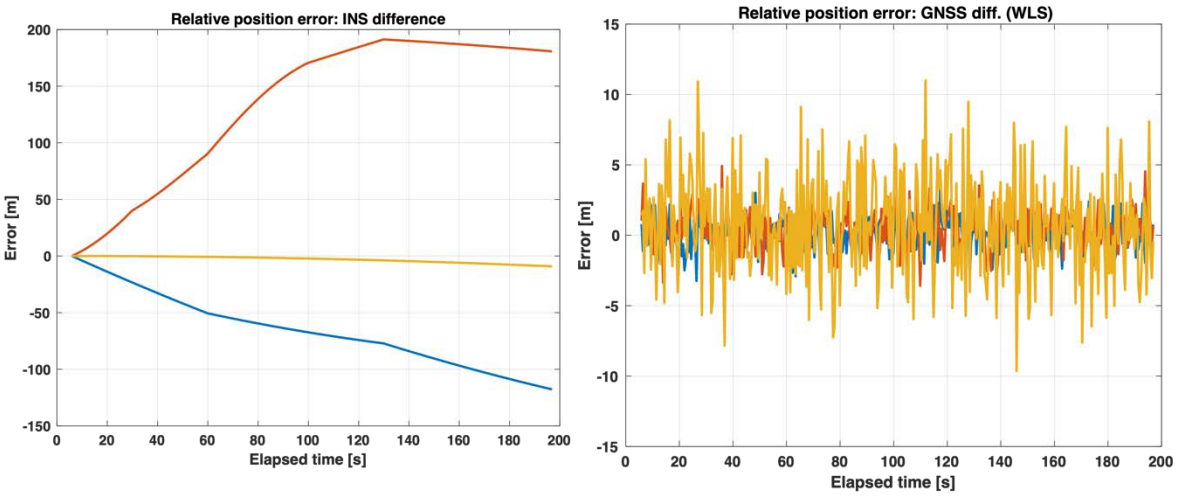

Figure 5-2: Separation vector errors: difference of INS positions (left) and GNSS-standalone estimates (right); blue: East-direction, red: North-direction, orange: up-direction.

To get rid of spatially correlated errors, SBAS corrections could be used. The resulting WLS solution is shown in Figure 5-3 (left). Although these results look very similar to the standalone GPS results, the position bias error here is close to zero unlike the GPS position.

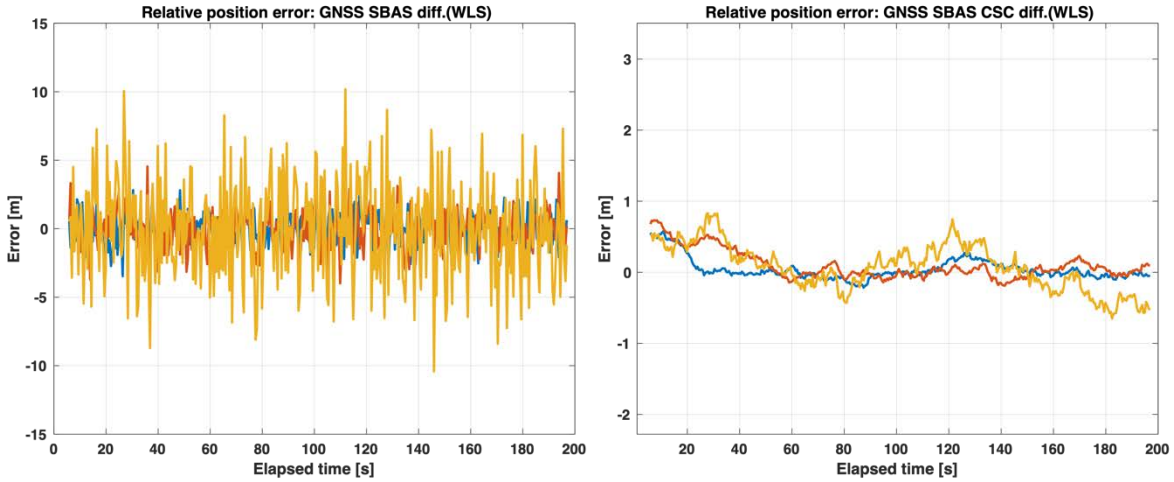

Figure 5-3: Separation vector errors: difference of SBAS pseudorange-only positions (left) and SBAS CSC solution (right). blue: East-direction, red: North-direction, orange: up-direction

Once we furthermore apply CSC according to equation (13), the results get much less noisy (see Figure 5-3 right). However, the vertical error is still large. This can be attributed to the geometry of the satellite resulting in a relatively large VDOP (visible were only 5-7 satellites with elevations larger than 25 degrees). Augmentation with an altimeter would result in a much better vertical reference and has been shown to significantly improve the vertical in [34]. One of the advantages of SBAS is that we can use the inherent built-in integrity to achieve higher levels of integrity of our solution.

Figure 5-4 shows the separation vector errors when using the method depicted in Figure 4-2 with (right) and without (left) CSC. Although the noise levels are slightly lower than SBAS, the advantage of this method is that no integrity information from SBAS is required, but that a modified version of RAIM can be applied to assess the integrity. Again, the vertical could be improved by augmenting with an altimeter using a WLS or EKF. Once the vertical error is reduced, there would be sufficient accuracy to line up with the platform. Another major advantage of the Figure 4-2 method is, that the velocity results are excellent. Accuracies of 4-8 mm/s can have been demonstrated in-flight [3].

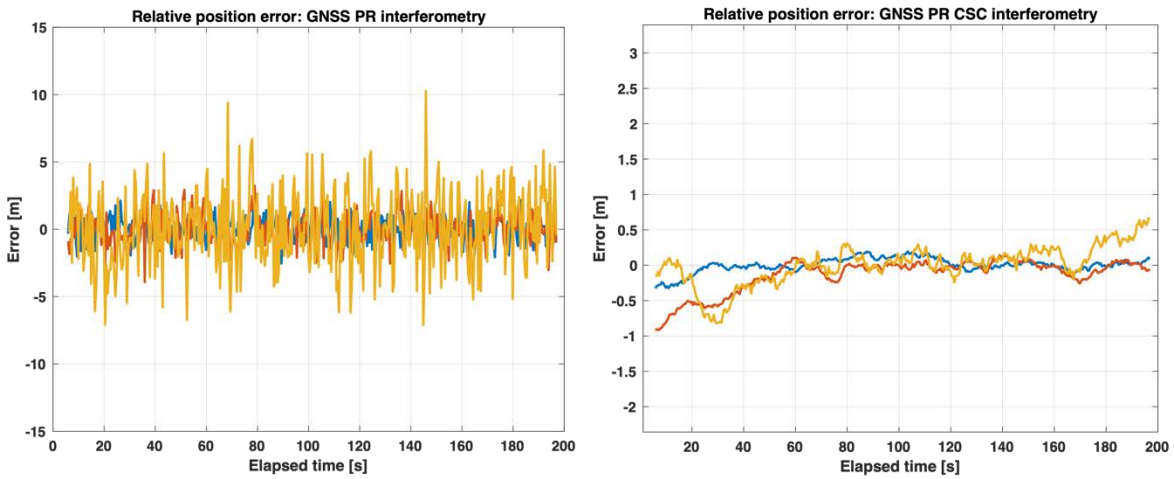

Figure 5-4: Separation vector errors: difference of INS positions (left) and GNSS-standalone estimates (right).

Not shown here are the RTK results. As they are solely based on carrier-phase measurements they have far better accuracies than the results of Figure 5-3 and 5-4. However, they would require a ground station. Of course, one could also apply ambiguity resolution to the method shown in Figure 4-2, but that approach was not implemented here.

In case we use solely RR measurements from the UWB beacons on the UGV, the results of Figure 5-5 are obtained. Note that the errors were chosen to be more pessimistic than the results shown in 4-3, but more optimistic operating ranges were chosen (way beyond 10m).

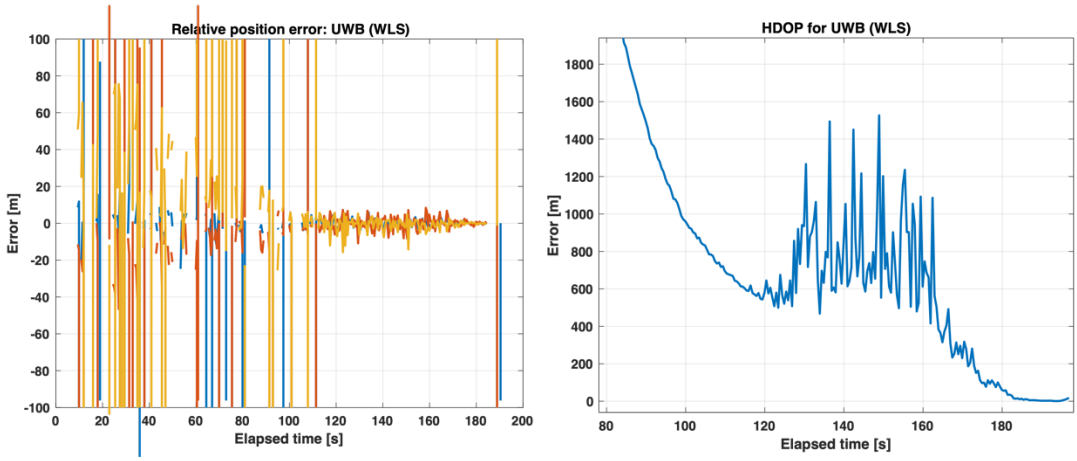

Figure 5-5: Separation vector errors: using UWB RR WLS (left) and HDOP (right).

As can be seen in Figure 5-5 on the left, the WLS estimator has a hard time converging. This is due to the very bad geometry at larger distances. This is obvious from the HDOP plot in Figure 5-5 on the right. Not until very late in the scenario when the distance falls below 6-7m, do we get lower and acceptable HDOPs. The bad geometry is in part caused by the close vicinity of the UWB antennas to one another due to the limited space on the UGV. Larger baselines would help but have not been evaluated.

To improve the method's convergence, another solution was implemented using a non-linear solver as the ones present in Matlab. The results are provided in Figure 5-6 and show better convergence, but still large errors as expected. The clipping in the vertical is due to the bounds defined in the solver.

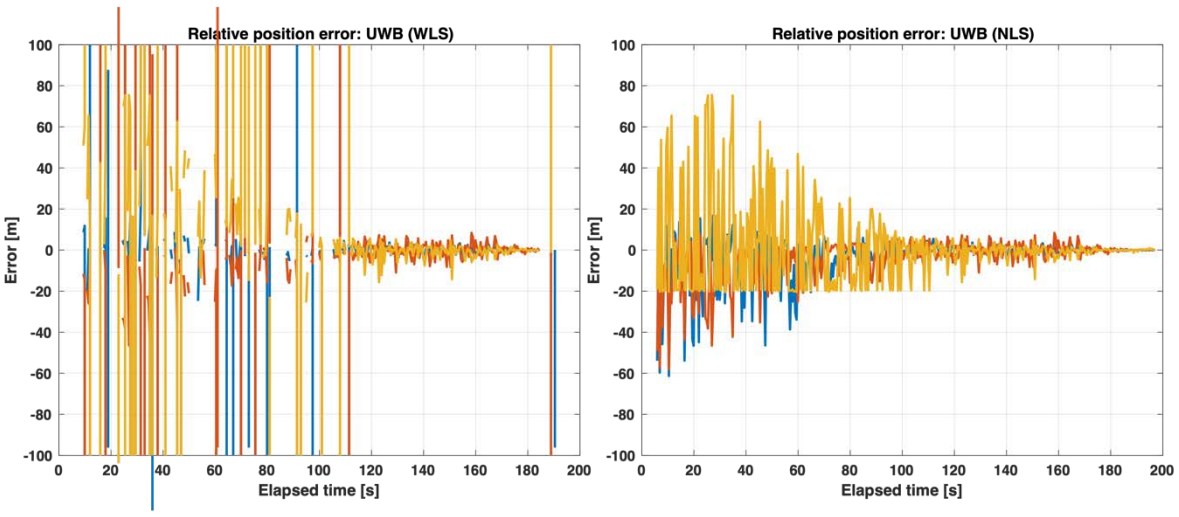

Figure 5-6: Separation vector errors: using UWB RR non-linear solver (left) and HDOP (right).

Finally, Figure 5-7 shows the results when incorporating the altitude measurement in the WLS solution. A significant reduction in error can be observed with even acceptable levels when getting close to the landing pad. This method could be sufficient to get close enough to transition to even a smaller marker-based guidance method.

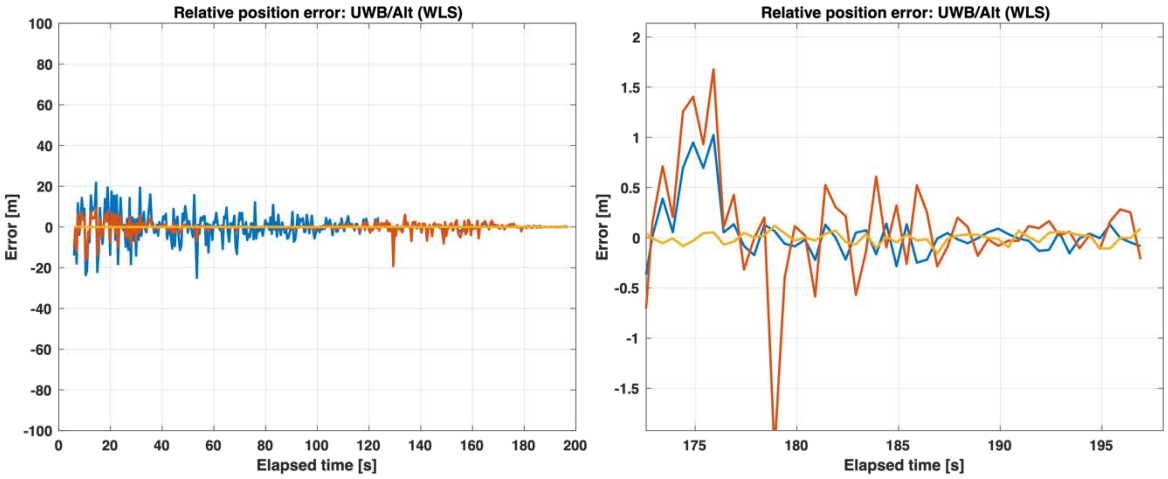

Figure 5-7: Separation vector errors: using UWB RR non-linear solver (left) and HDOP (right).

Another approach that is expected to be further reduced the noise is the integration with IMU. This approach is currently being developed and is outside the scope of this paper.

5.0 SUMMARY AND CONCLUSIONS

This paper provided an overview of methods that can be used to perform relative navigation between a UAV and a moving UGV supporting the final approach and lading phases of the flight. The paper introduced a general approach taken by the authors to solve this problem and that allows for several methods to be incorporated. The paper furthermore introduced a RR-based and RR/altimeter-based solution as an alternative way to support navigation during the landing phase. Simulation results were shown to illustrate what accuracies can be achieved by some of the discussed approaches and which ones would be sufficient for the approach and lading application. It was shown that RR-based methods can be used for this application but do require augmentation (altimeter or even inertial) to obtain dm-level accuracies during the final 10m. These simulations laid the foundation for the actual implementation on the TU Berlin UAV and UGV. The UAV and UGV platforms were described as well, and the next steps will be to finalize the hardware designs and flight test some of the proposed methods.

6.0 REFERENCES

[1] J. Coffey, “NOAA Unmanned Aircraft Systems (UAS) Program Activities,” *NOAA Briefing*, July 2014.

[2] RTCA SC-186, “Minimum Aviation System Performance Standards (MASPS) for Automatic Dependent Surveillance-Broadcast (ADS-B),” RTCA/DO-242A, Washington, DC, June 25, 2002.

[3] P. Duan, M. Uijt de Haag, J. L. Farrell, “Flight Test Results of a Measurement-Based ADS-B System for Separation Assurance,” *NAVIGATION*, Volume 60, Number 3, Fall 2013.

[4] J. Huff, A. Schultz, M. Uijt de Haag, "Assured Relative and Absolute Navigation of a Swarm of Small UAS," Proceedings of the IEEE/AIAA 36th Digital Avionics Systems Conference (DASC), St. Petersburg, FL, September 2017.

[5] T. Muskardin, et al., “Landing of a fixed-wing uav on a mobile ground vehicle,” Proceedings of the 2016 IEEE International Conference on Robotics and Automation (ICRA), Stockholm, Sweden, 2016.

[6] S. Bisnath, “Relative Positioning and Real-Time Kinematic (RTK)”, Chapter in Position, Navigation, and Timing Technologies in the 21st Century - Position, Navigation, and Timing Technologies in the 21st Century (editors Y. Morton et al.), Wiley IEEE Press, 2020.

[7] Farrell, J. L., *GNSS Aided Navigation & Tracking – Inertially Augmented or Autonomous*, American Literary Press, 2007.

[8] M. M. Miller, M. Uijt de Haag, A. Soloviev, M. Veth, “Navigating in Difficult Environments: Alternatives to GPS – 1,” Proceedings of the NATO RTO Lecture Series on “Low-Cost Navigation Sensors and Integration Technology,” SET-116, November 2008.

[9] M. M. Miller, J. Raquet, M. Uijt de Haag, “Navigating in Difficult Environments: Alternatives to GPS – 2,” Proceedings of the NATO RTO Lecture Series on “Low-Cost Navigation Sensors and Integration Technology,” SET-116, November 2008.

[10] K. Pluckter and S. Scherer, “Precision UAV Landing in Unstructured Environments,” Proceedings of International Symposium on Experimental Robotics (ISER '18), pp. 177 - 187, November 2018.

[11] E. Olson, “Apriltag: A robust and flexible visual fiducial system,” Proceedings of the 2011 IEEE International Conference on Robotics and Automation (ICRA), 2011.

[12] S. Garrido-Jurado, et al., “Automatic generation and detection of highly reliable fiducial markers under occlusion,” *Pattern Recognition*, 47(6), 2014.

[13] B. Benligiray, C. Topal, and C. Akinlar, “STag: A stable fiducial marker system,” *Image and Vision Computing*, vol. 89, pp. 158–169, Sept. 2019.

[14] M. Kalaitzakis, et al., “Experimental Comparison of Fiducial Markers for Pose Estimation,” *Proceedings of the 2020 International Conference on Unmanned Aircraft Systems (ICUAS*), Athens, Greece, 2020.

[15] J. W. Kim, et al., “Outdoor Autonomous Landing on a Moving Platform for Quadrotors using an Omnidirectional Camera,” *Proceedings of the 2014 International Conference on Unmanned Aircraft Systems (ICUAS)*, Orlando, FL, May 2014.

[16] S. Lange, et al., "Autonomous Landing for a Multirotor UAV using Vision," Proceedings of the International Conference on Simulation, Modeling, and Programming for Autonomous Robots (SIMPAR), Venice, Italy, 2008.

[17] D. Falanga, et al., "Vision-based autonomous quadrotor landing on a moving platform," *Proceedings of the 2017 IEEE International Symposium on Safety, Security and Rescue Robotics (SSRR)*, Shanghai, China, 11-13 Oct. 2017.

[18] T. Baca, et al., "Autonomous landing on a moving vehicle with an unmanned aerial vehicle," *Journal of Field Robotics*, 4 January 2019.

[19] S. M. Chaves, et al., "NEEC research: Toward GPS-Denied Landing of Unmanned Aerial Vehicles on Ships at Sea," Naval Engineers Journal, Volume 127, Number 1, March 2015.

[20] A. Borowczyk, et al., "Autonomous Landing of a Multirotor Micro Air Vehicle on a High Velocity Ground Vehicle," *Proceedings of the IFAC*, 2017.

[21] A. Paris, B. T. Lopez, J. P. How, "Dynamic Landing of an Autonomous Quadcopter on a Moving Platform in Turbulent Wind Conditions," *Proceedings of the 2020 International Conference on Robotics and Automation (ICRA)*, May 2020.

[22] J. Bacik, et al., "Autonomous Flying with Quadcopters using Fuzzy Control and ArUco Markers," *Intelligent Service Robotics*, 10, 2017.

[23] M. Bhargavapuri, et al., Vision-based autonomous tracking and landing of a fully-actuated rotorcraft," *Control Engineering Practice*, Vol. 89, 2019.

[24] "Precision Landing and Loiter with IR-Lock," https://ardupilot.org/copter/docs/precision-landing-with-irlock.html, Accessed September 2021.

[25] A. Scheithauer, "3D Relative Position and Orientation Estimation for Rendezvous and Docking Applications Using a 3D Imager," M.S.E.E. Thesis, Ohio University, 2010.

[26] J. Huff and M. Uijt de Haag, "Navigation of Multiple sUAS using GNSS, Inertial and Range Radios,", *Proceedings of the ION Pacific Position, Navigation and Timekeeping Conference*, Waikiki, HI, 2019.

[27] Loco Positioning Deck, "https://www.bitcraze.io/products/loco-positioing-deck/," accessed September 2021.

[28] M. R. Endsley, "Toward a Theory of Situation Awareness in Dynamic Systems," *Human Factors*, 1995, 37(1).

[29] M. Kamel, M. Burri, R. Siegwart, "Linear vs. Nonlinear MPC for Trajectory Tracking Applied to Rotary Wing Micro Aerial Vehicles," *IFAC*, 50, 2017.

[30] Y. Feng, et al., "Autonomous Landing of a UAV on a Moving Platform using Model Predictive Control," *Drones*, 2, 34, 2018.

[31] A. Gelb, *Applied Optimal Estimation*, MIT Press, 1974.

[32] K. Kotinkar, "Development of a sUAS Navigation Payload with GNSS, Inertial Sensors and Ultra-wideband Transceivers for Swarm Applications," M.Sc. Thesis, TU Berlin, July 2020.

[33] E. Kaplan and C. Hegarty, *Understanding GPS/GNSS: Principles and Applications*, Artech-House, Third Edition (Gnss Technology and Applications Series), 2017.

[34] A. Videmsek, M. Uijt de Haag, Timothy Bleakley, "Radar Altimeter Aiding of GNSS for Precision Approach and Landing of RPA," *Proceedings of the AIAA ICNS Conference*, Herndon, VA, April 9-11, 2019.